

Defect-induced absorption-band-edge values in β -FeSi₂

C. H. Olk* and S. M. Yalisove

Department of Materials Science and Engineering, University of Michigan, Ann Arbor, Michigan 48109-1120

G. L. Doll

*Physics Department, GM Research and Development Center, General Motors Corporation,
30500 Mound Road, Box 9055, Warren, Michigan 48090-9055*

(Received 22 December 1994; revised manuscript received 9 March 1995)

We have acquired optical transmission data on epitaxial thin films of semiconducting iron disilicide grown by pulsed laser deposition. Analysis of defect densities shows that values of the optical band-gap energy are effective band gaps that are lowered from the intrinsic value by the existence of band tails in the density of states. We propose that this influence may account for the wide range of optical band-gap energies reported for this material. We also find that the energy width of the defect bands can affect the assignment of the nature of the band-gap transition.

I. INTRODUCTION

Semiconducting iron disilicide (β -FeSi₂) has drawn much attention in recent years.¹ Investigations of the electrical and optical properties have determined a range of 0.7–1.38 eV for the valence- to conduction-band separation.^{2–7} The intrinsic absorption edge is considered to be caused by allowed transitions from the silicon 3*p* band to the 3*d* band of iron.⁴ Theoretical studies of the band structure have predicted that the forbidden transition is indirect,^{8,9} with some disagreement on the value of the energy difference between the direct and indirect transitions. The majority of experimental findings suggest that the transition is direct in nature. A widely accepted value of the energy gap is 0.87 eV.³ Recently, separate reports of optical absorption on samples grown by conventional solid phase epitaxy¹⁰ and by ion-beam synthesis¹¹ presented evidence that the energy-gap transition is indirect. The exact value and nature of the intrinsic energy gap have yet to be determined, since all films produced to date contain structural imperfections that inevitably contribute to the electronic and optical properties. Since these properties will ultimately determine the merit of this material for electrical and optical applications, the affects of the structural imperfections require deliberate investigation.

It is well known that high concentrations of crystalline imperfections or defects (e.g., impurities, dislocations, bond defects, or grain boundaries) in semiconductor samples, usually polycrystalline and containing small grains, create tails in the distribution of the density of states.^{12–15} The reason for this is that as the distances between defects becomes small, their energy levels broaden into bands. These bands then merge with the nearest parent bands of the extended states. The results produce an effective energy gap. An example of a reduced energy gap due to exponential band tailing has been reported¹⁶ for fine grain polycrystalline silicon, in which the grain boundaries exhibit at 1.0-eV band gap that merges with the crystal band.

Although much is known about the general structure and epitaxy of β -FeSi₂, a wide range of values of specific physical properties has been reported. Several investigations of the optical properties^{2,3,11,12,17–20} of β -FeSi₂ have been performed, all of which report the existence of subgap absorption attributed to the presence of defect states within the forbidden region. Deep-level transient spectroscopy²⁰ provided evidence of two defect states with energies of 0.50 and 0.53 eV, determined to be located near the silicon silicide interface. A recent study²¹ of β -FeSi₂, grown by chemical vapor deposition, reported that despite nearly identical structural characteristics, as measured by Rutherford backscattering, x-ray diffraction, and transmission electron diffraction (TED), individual samples grown at different temperatures exhibited very different photoluminescence spectra. Furthermore, the results they reported differed significantly from photoluminescence spectra taken on samples grown by conventional solid phase epitaxy.² These, as well as a report of the existence of mixed phases present at the silicon-silicide growth interface over a wide range of temperature,^{22,23} suggest that a wide variety of individual sample characteristics result from a relatively narrow set of variations in growth parameters. Examination of the literature reveals that similarities of specific characteristics (e.g., composition, phase, epitaxy), do not necessarily lead to agreement in the assignment of many key physical quantities and properties (e.g., band-gap value and nature, resistivity, or conduction mechanism). In this paper we present an examination of optical-absorption data from which we calculate the defect state density and explore its relationship with the assigned band-gap value for samples with different grain sizes. We also discuss the determination of the nature of the energy-gap transition within the context of defect density.

II. SAMPLE PREPARATION

Samples were prepared by the stoichiometric codeposition of β -FeSi₂ ablated from a solid iron disilicide target

by a pulsed laser beam onto Si(111) substrates.²⁴ Pulsed laser deposition provides advantages over the conventional silicidation processes in that it does not require multistep deposition or interdiffusion via thermodynamic equilibrium between the film and substrate. Since no thermal annealing is required, we presume that no significant consumption of the underlying silicon substrate occurs. Targets of FeSi₂ and silicon were load-locked into the UHV (base pressure 2×10^{-10} torr) deposition chamber and were briefly ablated to remove surface contamination. Si(111) wafers were immersed in a 5% solution of HF acid and deionized water²⁵ for approximately 5 min, rinsed with deionized water, mounted on Mo substrate holders and then load-locked into the deposition chamber. The substrate was positioned 7 cm directly in front of the target, and the growth temperature range was 570–630°C. Light from a KrF excimer laser (248 nm) was focused to a spot (~ 2 mm²) on the FeSi₂ target at an incident angle of 45°. The incoming beam was rastered across the surface to avoid pitting of the targets.

We examined the substrates upon introduction to the growth chamber using *in situ* reflection high-energy electron diffraction (RHEED) with a beam energy of 15 keV and a grazing angle of about 1° directed along a Si<112> direction. Prior to any increase in temperature, the substrate exhibited a streaked 1×1 diffraction pattern indicative of a smooth surface on a scale at least as large as the coherence length (~ 10 nm) (Ref. 26) of the incident electrons. The silicon substrate was subsequently heated to approximately 600°C while exposing it to a silicon flux of several hundred laser pulses from a silicon target. This process produced a finely streaked 7×7 RHEED pattern. Ablation of the FeSi₂ target was carried out at 300–800 mJ with a 2–10-Hz repetition rate. At these repetition rates and energies the deposition of FeSi₂ ranged from 0.026 to 0.135 Å/pulse. During the growth process, the chamber pressure remained below 2×10^{-9} torr. The formation of β -FeSi₂ on the substrate results in a RHEED pattern similar to the initial 1×1 pattern of the silicon (111) substrate, but includes the addition of two intermediate streaks. This can be explained by the orientation of the β -FeSi₂ lattice which presents diffracting planes, parallel to the beam direction, with a separation that is twice that of the Si substrate. This pattern is observed throughout the entire growth, and remains after the sample is cooled to room temperature. Since we observed no diffraction spots with RHEED during film growth, we assume that there was no formation of three-dimensional islands.

We grew films with thicknesses ranging from 175 to 780 Å. *Ex situ* depth profiling by Auger spectroscopy and argon sputtering indicated that the films contained trace impurities of carbon and oxygen found within 30 Å of the film surfaces. Below 30 Å the films were stoichiometrically correct to within 10%, through the entire thicknesses. X-ray-diffraction results confirmed that these films are indeed orthorhombic β -FeSi₂. Transmission electron diffraction performed on our samples showed a fine grain (diameters 360–855 Å) polycrystalline morphology. Analysis of selected area diffraction

patterns for films of various thicknesses suggests that the epitaxial relationship is β -FeSi₂ (001)||Si(111). Details of the structural analysis of these films has been reported elsewhere.²⁷ This relationship has been previously produced by molecular-beam epitaxy (MBE),²⁸ and results in the smallest geometric misfit known for this material system. Furthermore, there exist three equivalent rotational variants aligned as β -FeSi₂ [010]||Si[$\bar{1}10$], β -FeSi₂ [010]||Si [10 $\bar{1}$], and β -FeSi₂ [010]||Si[0 $\bar{1}1$].

III. EXPERIMENTAL METHODS AND RESULTS

The optical measurements were made using a modified Perkin-Elmer Lambda 9 spectrometer. The spectrometer provides a dual-beam arrangement and incorporates a double monochromator in series in a Littrow configuration. For the range of energy (0.5–1.0 eV) over which data were acquired, a PbS detector was utilized. A tungsten-halogen lamp acts as the light source. The spectrometer was operated at room temperature in air. Although silicon is transparent to photons with energies in the range over which the data was acquired, we chose to

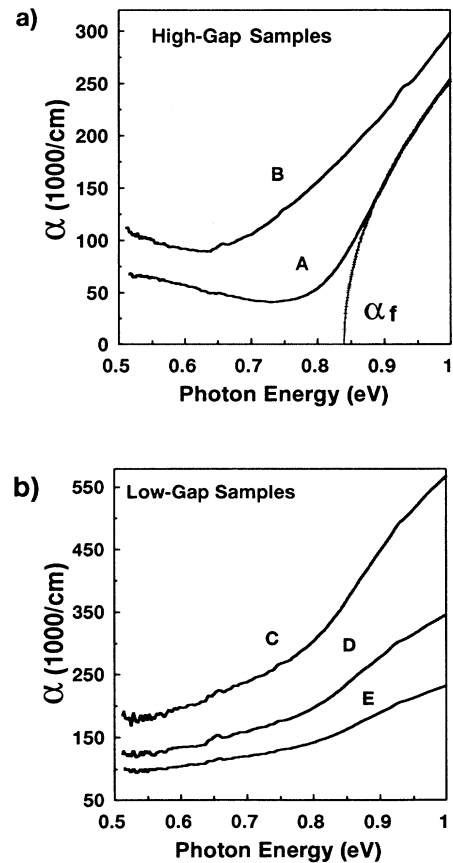


FIG. 1. Absorption coefficients vs photon energy for β -FeSi₂ grown by PLD. (a) High-gap samples and a fit to the direct-gap model. (b) Low-gap samples. The average grain diameters are 855 and 725 for samples A and B and 360, 465, and 490 (± 50) Å for samples C, D, and E, respectively.

utilize a dual background correction function that allowed subtraction of the contribution to the transmission data by the substrate. This operation stores the correction values necessary to produce data that show the absorption in the iron disilicide film without subband features due to the silicon substrate.

Owing to the high refractive index ($n = 5.6$) of β -FeSi₂ (Ref. 29) and very low values of the transmission over the photon energy range probed, interference and reflection effects can be neglected thus allowing the simplified expression for the absorption coefficient, $\alpha = -\ln(I)/t$ (t is the film thickness), to be applied. The absorption coefficient for two sets of samples are shown in Fig. 1(a) (sample *A*, $t = 720$ Å; sample *B*, $t = 780$ Å) and 1(b) (sample *C*, $t = 175$ Å; sample *D*, $t = 330$ Å, sample *E*, $t = 500$ Å). We have confined our discussion to three general features of the absorption coefficients, the specific values of which are determined for each sample: the region from near midgap (~ 0.5 eV) to the minimum in the absorption coefficient (E_{α}^m), the exponential region from E_{α}^m to the assigned value of the effective band gap (E_g^e), and a region a few hundred eV on either side of E_g^e . The exponential region is characterized by an energy-dependent rise in α of several orders of magnitude, and obeys Urbach's rule.³⁰ There is a general agreement that characteristic features of this region are a measure of the structural disorder of the material. The Urbach edge may arise as a consequence of fields associated with ionized impurities, charged defects, or photon-induced microfields.³¹ Although other common specific structural features appear within the spectra, we will not attempt to explain their origin.

The curves (*A* and *B*, high-gap samples) of Fig. 1(a), clearly show minimums in the absorption coefficient between 0.5 eV and the absorption edge. The rise in the absorption coefficient as the photon energy is lowered from E_{α}^m , to α at 0.5 eV, has been associated with midgap defect states.^{2,3,20} While it exists, E_{α}^m is much less apparent in the low-gap samples, curves *C*, *D*, and *E*, of Fig. 1(b), but can be identified in the numerical data. The values of the absorption coefficients for all samples are in the 1×10^5 (cm⁻¹) range which is typical for β -FeSi₂.

The nature of the band gap can be determined by fitting the absorption data to theoretical curves that follow the relationships³²

$$\alpha(h\nu) = A(h\nu - E_g^d)^{1/2} \quad (1)$$

in the case of a solid with a direct gap, and

$$\alpha(h\nu) = A'(h\nu - E_g^{\text{id}} - E_{\text{ph}})^2 \quad (2)$$

in the indirect-gap case. The indirect equation contains the energy associated with the creation of a phonon E_{ph} . The constants A and A' are associated with specific details of the band structure. In Fig. 2, an extrapolation to $\alpha = 0$ of the linear part of the absorption curves using the above expression are made for high-gap samples *A* and *B* and low-gap samples *C*–*E*. A tentative fit to direct as well as indirect gaps can be made for the high-gap sample *A*. The confidence with which we assign an indirect nature and gap value to sample *A* is low. Nevertheless, the fits of the curves in Figs. 2(a) and 2(c) show that the absorption coefficient of two separate samples can be interpreted in a manner that assigns an indirect nature to the

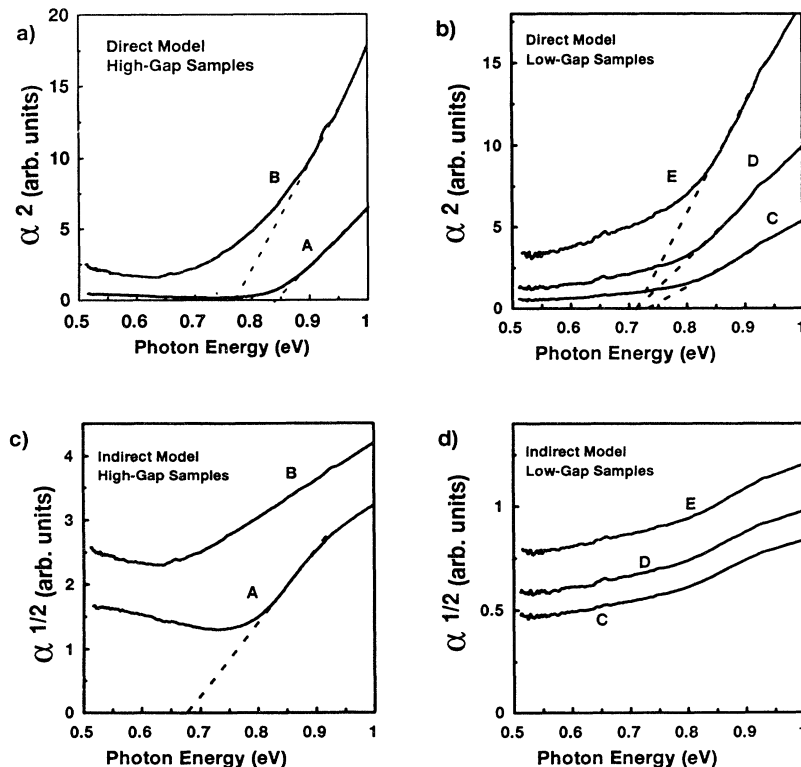


FIG. 2. Plots of and fits (dashed lines) to the square of the absorption coefficients for (a) high-gap and (b) low-gap samples. The square root of the absorption coefficients for (c) high-gap and (d) low-gap samples.

energy-gap transition in one though not in the other. It is this anomaly in our data coupled with the conflicting assignments of the nature as well as value of the band gap thus far reported in the literature that has motivated this work. To the best of our knowledge, assignments of the nature and value of the gap in β -FeSi₂, based on optical absorption, have been made without extensive consideration as to how the defect density may alter the shape of the absorption curve.

The $E_{ph} + E_g^{id} = 0.68$ -eV value assigned to sample *A* by the fit to the indirect model Eq. (2), Fig. 2(c), is quite a bit lower than the sum $E_{ph} + E_g^{id} = 0.78$ assigned to the indirect-band gap for samples in [11]. The low-gap samples (*C*, *D*, and *E*) can be assigned direct-gap values as shown in Fig. 2(b), while no indirect values can be assigned to these samples. The assigned energy-gap values are listed in Table I.

It is well known that the presence of high concentrations of crystalline imperfections cause band tailing that result in an extension of the distribution of the density of states into the forbidden energy region.³³ Three possible causes of band tailing have been identified by Pankove:³⁴ (1) The spatial overlap of defect energy levels broadens into a band that merges with the nearest intrinsic band. (2) The accommodation of defects by the lattice results in localized strains, producing a deformation potential that locally alters the energy gap. This effect smears the band edges, and the effective gap is a superposition of locally induced gap values of various energies. (3) Ionized defects exert forces on the charge carriers and on the associated band, thereby smearing the band edges. In Fig. 3(a), a simple band picture shows the cumulative effect of the above causes. Since our samples are *p* type, as determined from transport experiments,³⁵ this diagram schematically represents the transitions that link delocalized states in the parabolic valence band to localized states near the conduction band. The term E_g^i is the value of the intrinsic energy gap to which we have assigned 0.84 eV for comparative purposes; it is the highest gap value we obtained for our samples. The effective energy gap (E_g^e) is the value we assigned to each sample based on fits to the direct transition model Eq. (1). E_g^e is shown in Fig. 3 to be the result of bands formed from localized states merging with the parent bands of the intrinsic crystal. E_α^m is the energy value at which a

minimum in the absorption coefficient occurs due to the decrease in the density of localized states at energies too far from the intrinsic band edge to merge with it. We presume that for energies less than E_α^m there are few defect states that will affect the assignment of the value or nature of the band gap. The location of E_α^m , E_g^e , and E_g^i are shown in Fig. 3(b), in a schematic diagram of the absorption spectrum.

If the band gap for β -FeSi₂ is affected by the presence of band tails, one would expect a positive correlation between the number of defects and the assignment, from optical-absorption coefficients, of the value and nature of the band gap. The excess optical absorption α_{ex} , due to subgap states, can be computed from

$$\alpha_{ex} = \alpha - \alpha_f, \quad (3)$$

where α_f can be an exponential fit³⁶ to the absorption coefficient of the highest gap sample made in a region just below the assigned gap energy. This fit would include the absorption due to defects and hence the band tail associated with the density of localized states of this intrinsic

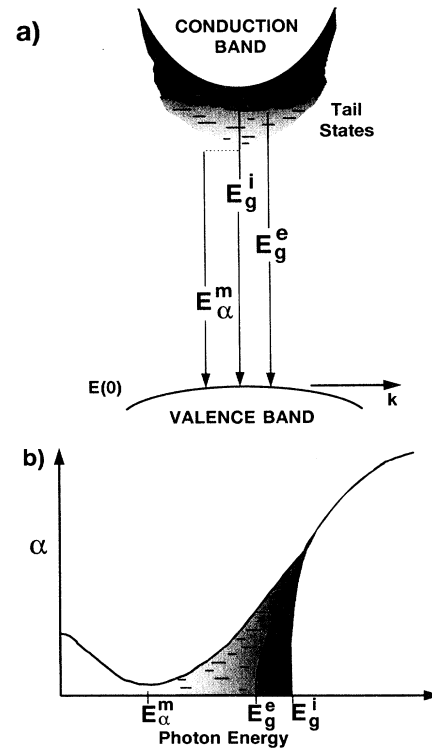


TABLE I. Properties of PLD samples of β -FeSi₂. N_0 is the calculated defect density. The surface-to-volume ratio is proportional to the inverse grain diameter (d). The energy-gap values are taken from appropriate fits to the absorption curves.

Sample	N_0 (cm ⁻³) E_α^m thru $E_g^i = 0.84$ eV	Surface/Volume $\propto (1/d)$ ($10^3 \times \text{\AA}^{-1}$)	Optical energy gap (eV) and nature
A	2.4×10^{18}	1.17	0.84 direct 0.68 indirect
B	1.0×10^{19}	1.38	0.78 direct
E	1.6×10^{19}	2.04	0.72 direct
D	2.0×10^{19}	2.15	0.72 direct
C	3.2×10^{19}	2.78	0.73 direct

FIG. 3. (a) Simple band picture indicating band formation from broadened energy levels (—) of defects, and their subsequent merger with the parent energy bands resulting in an effective band gap E_g^e . The intrinsic band gap is E_g^i and E_α^m is the lowest absorbing energy near the band edge and produces a minimum in the absorption coefficient. States usually found near the midgap are not depicted. (b) The location of E_α^m , E_g^e , and E_g^i are shown in a schematic diagram of the absorption spectrum. The midgap absorption is shown here in order to resemble an actual spectrum.

sample. Alternatively, a fit determined by Eq. (1) [$\alpha_f = A(h\nu - E_g^i)^{1/2}$] describing ideal intrinsic absorption of the highest gap sample at the band edge may be used. Since quantitatively similar results were produced using each fitting procedure, the following considerations seemed appropriate. The use of the exponential fit and subsequent subtraction would presume a near-intrinsic character for our best sample. However, since our best sample has a gap energy that is significantly lower than many previously reported values, it most likely contains defects that affect the assignment of the band-gap energy and nature. We therefore have chosen to report results of the second procedure, since in doing so α_{ex} will include absorption by states near the band edge of all samples. The fit utilized is plotted in Fig. 1(a). The calculated excess absorption coefficients, Eq. (3), are shown in Figs. 4(a) and 4(b).

The defect density can be calculated from³⁷

$$N_0 = 8.21 \times 10^{16} \left[\frac{n}{(n^2 + 2)^2} \frac{1}{f_{oj}} \right] \int \alpha_{ex} dE, \quad (4)$$

where the numerical prefactor contains the speed of light, the mass and charge of the electron, and Planck's constant; $n (= 5.6)$ is the refractive index,²⁷ and f_{oj} is the oscillator strength of the absorption transition. Assuming $f_{oj} = 1$ we obtain a combined prefactor of 4.13×10^{14} . Defect densities are calculated from Eq. (4) by integrating

α_{ex} over the energy range E_α^m through $E_g^i = 0.84$ eV (the highest gap value found for our samples). Equation (4) produces the values given in Table I. These results clearly distinguish the high-gap from the low-gap sample groups.

IV. SUMMARY

Results (Table I) show much lower densities of defects in samples that can be assigned relatively high-gap energies ($N_0 \leq 10^{19} \text{ cm}^{-3}$) than in those assigned low-gap energies ($N_0 > 10^{19} \text{ cm}^{-3}$). By comparison, samples grown by solid phase epitaxy with an energy-gap value of 0.85 eV were reported to contain a defect density of $\sim 10^{19} \text{ (cm}^{-3}\text{)}$.² The defect density we calculated for sample *A*, which has nearly the same gap value, is $2.4 \times 10^{18} \text{ cm}^{-3}$. Using TEM dark field images an estimate of the average grain size was calculated for each sample. Samples *A* and *B* possess very similar average grain diameters (*A*, $d = 855$; *B*, $d = 725$ Å), while the grains sizes of samples *C*, *D*, and *E* are significantly smaller (*C*, $d = 360$; *D*, $d = 465$; *E*, $d = 490$ Å). Assuming cylindrical geometry for the grains, we calculated the surface-to-volume ratios shown in Table I, and plot these values versus defect densities in Fig. 5. From the plot the correlation between the increase in the density of defects with the increase in the surface-to-volume ratio can be seen. This correlation suggests that the majority of localized states exist as defects at the grain boundaries. This seems reasonable, since the grains are formed in one of three equiprobable equivalent rotational variants that present high-index planes to each other. The properties of the atoms in the grain boundary are expected to be very different from those within the grains, since the bonding configurations are likely to be substantially modified. Further investigations such as electron-spin resonance are required to determine the exact nature of the grain-boundary defects.

From our results it appears likely that any assignment of a value or nature to the band-gap transition in $\beta\text{-FeSi}_2$, based on optical-absorption data, can be somewhat presumptuous since the spectra are complicated by the presence of high defect densities. We find that the

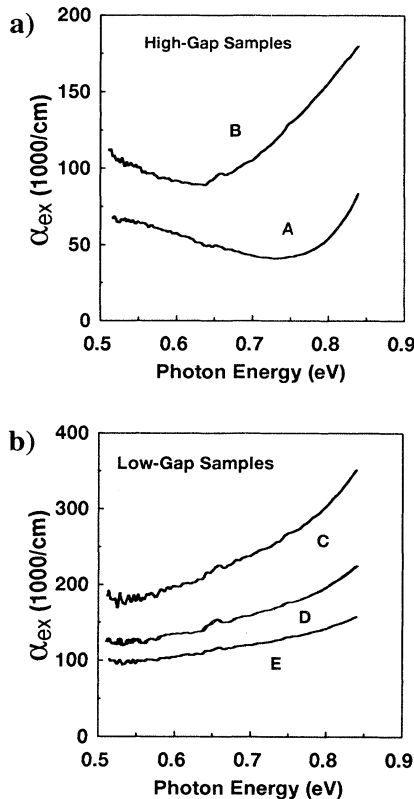


FIG. 4. The calculated defect-related excess absorption coefficients for (a) high-gap and (b) low-gap samples. The values of the defect densities are given in Table I.

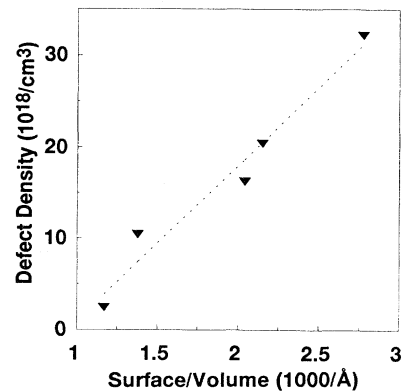


FIG. 5. A plot of the defect density vs the idealized cylindrical grain surface-to-volume ratio ($\propto 1/\text{diameter}$).

difference between the lowest and highest effective energy gaps in our samples is 0.12 eV, a value that is close to the measured difference between the indirect and direct transition energy levels found for sample *A* (0.16 eV). Since an assignment of an indirect nature can only be made for sample *A* ($N_0 < 1 \times 10^{19} \text{ cm}^{-3}$), and a fit of the indirect model to the optical absorption of sample *B* ($N_0 = 1 \times 10^{19} \text{ cm}^{-3}$) is unconvincing, we presume that a defect density greater than $1 \times 10^{19} \text{ cm}^{-3}$ produces a smearing of the band edge by an energy amount near or greater than the difference between direct- and indirect-gap energies in β -FeSi₂. Support for this conclusion comes from results of an optical-absorption study of β -FeSi₂ samples grown by ion-beam synthesis¹¹ that reported an indirect-band gap value of 0.78 eV and a direct value of 0.90 eV. The difference of 0.12 eV is quite near the difference for our sample *A*. Although they did not report a defect density, they did report a mobility of 104 (cm²/V s). Typical mobility values for β -FeSi₂ are 1–10 (cm²/V s). An order-of-magnitude higher mobility suggests that their crystalline perfection should be higher than films produced by PLD or by more conventional methods.

In conclusion, we find that the existence of high defect densities in β -FeSi₂ can produce band tails with an apparent energy width near the value of the measured difference between the indirect and direct transition energy levels. The band tails merge with the parent bands, thereby altering the intrinsic band structure, the results of which is an assigned effective direct band-gap energy lower than the expected intrinsic value. From our results, and others that used a variety of growth conditions and methods, we suggest that the existence of band tails in the density of states of β -FeSi₂ and the subsequent alteration of the optical absorption may preclude the assignment of an indirect nature to the band-gap transition in samples containing them. Furthermore, we find that in samples with few enough defects, an indirect nature can be assigned to the band-gap transition of β -FeSi₂, in agreement with theoretical predictions.

ACKNOWLEDGMENTS

The authors thank O. P. Karpenko for contributions necessary to these results. We also thank Dr. J. P. Heremans for useful discussions.

*Present address: Physics Department, NAO R&D Center, General Motors, Warren, MI 48090.

¹J. Derrien, J. Chevrier, V. Le Thanh, J. Berbezier, C. Giannini, S. Lagomarsino, and M. G. Grimaldi, *Appl. Surf. Sci.* **73**, 90 (1993), and references therein.

²C. A. Dimitriadis, J. H. Werner, S. Logothetidis, M. Stutzmann, J. Weber, and R. Nesper, *J. Appl. Phys.* **68**, 1726 (1990).

³M. C. Bost and J. E. Mahan, *J. Appl. Phys.* **58**, 2696 (1985).

⁴H. P. Geserich, S. K. Sharma, and W. A. Theiner, *Philos. Mag.* **27**, 1001 (1973).

⁵U. Birkholz and J. Naegele, *Phys. Status Solidi* **39**, 197 (1970).

⁶U. Birkholz and J. Schelm, *Phys. Status Solidi* **27**, 413 (1968).

⁷R. M. Ware and D. J. McNeill, *Proc. IEEE* **111**, 178 (1964).

⁸N. E. Christensen, *Phys. Rev. B* **42**, 7148 (1990).

⁹R. Eppenga, *J. Appl. Phys.* **68**, 3027 (1990).

¹⁰C. Giannini, S. Lagomarsino, F. Scarinci, and P. Castrucci, *Phys. Rev. B* **45**, 8822 (1992).

¹¹K. Radermacher, R. Carius, and S. Mantl, *Nucl. Instrum. Methods Phys. Res. Sect. B* **84**, 163 (1993).

¹²D. Redfield, J. P. Wittke, and J. I. Pankove, *Phys. Rev. B* **2**, 1830 (1970).

¹³H. Kressel and J. K. Butler, *Semiconductor Lasers and Heterojunction LED's* (Academic, New York, 1977), p. 18.

¹⁴W. B. Jackson and N. M. Amer, *Phys. Rev. B* **25**, 5559 (1982).

¹⁵C. A. Dimitriadis, D. H. Tassis, N. A. Economou, and G. Giakoumakis, *Appl. Phys. Lett.* **64**, 2709 (1994).

¹⁶W. B. Jackson, N. M. Johnson, and D. K. Biegelsen, *Appl. Phys. Lett.* **43**, 195 (1983).

¹⁷M. Powalla and K. Herz, *Appl. Surf. Sci.* **70/71**, 593 (1993).

¹⁸K. Lefki, P. Muret, N. Cherief, and R. C. Cinti, *J. Appl. Phys.* **69**, 352 (1991).

¹⁹T. D. Hunt, K. J. Reeson, K. P. Homewood, S. W. Teon, R.

M. Gwilliam, and B. J. Sealy, *Nucl. Instrum. Methods Phys. Res. Sect. B* **84**, 168 (1993).

²⁰E. K. Evangelou, G. E. Giakoumakis, and C. A. Dimitriadis, *Solid State Commun.* **86**, 309 (1993).

²¹J. L. Regolini, F. Trincat, I. Sagnes, Y. Shapira, G. Bremond, and D. Bensahel, *IEEE Trans. Electron Devices* **ED-39**, 200 (1992).

²²F. Sirotti, M. DeSantis, X. Jin, and G. Rossi, *Phys. Rev. B* **49**, 11 134 (1994).

²³H. Moritz, B. Rosen, S. Popovic, A. Rizzi, and H. Luth, *J. Vac. Sci. Technol. B* **10**, 1704 (1992).

²⁴C. H. Olk, O. P. Karpenko, S. M. Yalisove, and G. L. Doll, *J. Mater. Res.* **9**, 324 (1994).

²⁵M. Grundner and H. Jacob, *Appl. Phys. A* **39**, 73 (1986).

²⁶E. Bauer, in *Interactions on Metal Surfaces*, edited by R. Groma, Topics In Applied Physics Vol. 4 (Springer, Berlin, 1975), p. 225.

²⁷O. P. Karpenko, C. H. Olk, G. L. Doll, S. M. Yalisove, and J. F. Mansfield, *J. Appl. Phys.* **76**, 2202 (1994).

²⁸H. Sirringhaus, N. Onda, E. Muller-Gubler, P. Muller, R. Stalder, and H. Vonkanel, *Phys. Rev. B* **47**, 10 567 (1993).

²⁹M. C. Bost and J. E. Mahan, *J. Appl. Phys.* **64**, 2034 (1988).

³⁰F. Urbach, *Phys. Rev.* **92**, 1324 (1953).

³¹J. D. Dow and D. Redfield, *Phys. Rev. B* **5**, 594 (1972).

³²J. J. Pankove, *Optical Processes in Semiconductors* (Dover, New York, 1971), p. 36.

³³R. H. Parmenter, *Phys. Rev.* **97**, 587 (1955).

³⁴J. I. Pankove, *Phys. Rev.* **140**, A2059 (1965).

³⁵C. H. Olk, S. M. Yalisove, J. Heremans, and G. L. Doll (unpublished).

³⁶J. Tauc, *Mater. Res. Bull.* **3**, 37 (1968).

³⁷D. L. Dexter, *Phys. Rev.* **101**, 48 (1956).

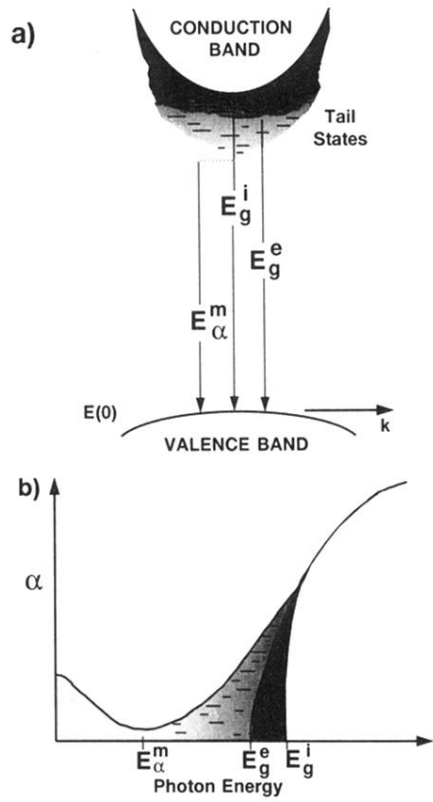


FIG. 3. (a) Simple band picture indicating band formation from broadened energy levels (—) of defects, and their subsequent merger with the parent energy bands resulting in an effective band gap E_g^c . The intrinsic band gap is E_g^i and E_α^m is the lowest absorbing energy near the band edge and produces a minimum in the absorption coefficient. States usually found near the midgap are not depicted. (b) The location of E_α^m , E_g^e , and E_g^i are shown in a schematic diagram of the absorption spectrum. The midgap absorption is shown here in order to resemble an actual spectrum.